

Accepted for publication in the J. Acoust. Soc. Am., March 3, 2000

# Effects of interaction between two bubble scatterers

George Kapodistrias

Department of Mechanical Engineering and Applied Physics Laboratory  
University of Washington, Seattle, WA 98195

Peter H. Dahl

Applied Physics Laboratory  
University of Washington, 1013 NE 40th Street, Seattle, WA 98105

## Abstract

The backscattering of sound from two regularly arranged bubbles is studied theoretically and experimentally. In well-controlled laboratory experiments a bistatic acoustic system is used to interrogate the scatterers, which are placed on a very fine thread at the same distance  $d$  from the combined beam axis of the set of transmitting and receiving transducers. The radius of each bubble is  $585 \mu\text{m}$ . The frequency range is 80–140 kHz, and  $d$  is varied so that the variable  $kd$  spans the range 0.2–21, where  $k$  is the acoustic wavenumber. Scattering calculations are carried out using an exact, closed-form solution derived from the multiple scattering series. Several experiments are performed, and the results are in close agreement with the calculations. It is verified that multiple scattering induces an oscillatory behavior about the exact coherent scattering level, with decreasing amplitude for increasing  $kd$ . For interbubble distance  $2d \approx \lambda/2$  the backscattered radiation is maximized, while for  $2d < \lambda/2$  the radiation is reduced considerably. These and other effects are discussed.

## Introduction

Understanding the physical processes that develop when sound traverses through and scatters from a dense assemblage of scatterers is of great importance in a number of applications, such as scattering from oceanic bubble clouds [1], schools of fish [2], plankton [3], ultrasonic contrast agents [4], and blood [5]. In such cases, multiple scattering complicates the inverse scattering problem of extracting information about the scatterers or the scattering medium from the acoustic field at the receiver. In this paper, we address a component of the forward problem pertaining to multiple scattering. The fundamental question we seek to answer is how the backscattered wave is affected by varying the center-to-center distance,  $2d$ , between two bubble scatterers symmetrically arranged about the combined beam axis. Subsequent discussions and analysis will refer to air bubbles in water, although the general theory is not restricted to such.

Consider an assemblage of bubbles with mean inter-bubble distance  $2d$ , insonified by a plane wave with wavelength  $\lambda$ . For a sparse assemblage of bubbles, say  $2d \gg \lambda$ , that are randomly spaced (as could be the case for some oceanic bubble clouds), the possibility of interaction between the individual bubbles is small, and multiple scattering effects can be neglected (e.g., see Morse and Ingard [6]). Therefore, the Born approximation is valid, and it can be shown that the total (incoherent) scattered intensity per unit incident intensity at a point in the field assumes a linear dependence between the number of bubbles and their total scattering cross section. However, for regularly spaced (and sparse) assemblages the total intensity at the receiver is the result of coherent scattering, and is therefore equal to the square of the sum of the individual scattered pressures. For dense assemblages, say  $2d \leq \lambda$  (as could be the case for bubble clouds very close to the surface or those associated with surf zones), the theoretical analysis is more complicated, because the interactions between the bubbles play a definite role in the development of the scattered field. These interactions include, among others, multiple scattering.

In multiple scattering the field scattered from each element depends both on the incident wave from the source and on the waves scattered by all other elements in the scattering

volume. It is possible to write a series of scattering terms to obtain the acoustic field at the receiver. However, this series is infinite and also will become quite intractable for a large number of scatterers. One approach that simplifies the problem is to perform a partial summation on only the most important contributions to the series (e.g., see Refs. [7] and [8]). Another simplification that incorporates multiple scattering effects is to treat the volume occupied by the bubbles as a continuous one with some equivalent density and compressibility. Such a solution, offered in 1945 by Foldy [9], is the “effective medium” model. This approach is based on averaging the acoustic field scattered by a large number of omnidirectional scatterers governed by a spatial Poisson distribution. Since then other researchers have improved on Foldy’s effective medium model by adding small corrections [10], [11], [12]. The effective medium approximation has been successfully compared with experimental data from random assemblages for insonifying frequencies that do not correspond to the resonance frequency of the bubbles. For example, Commander and Prosperetti [1] used the model to analyze five different data sets, and the results showed good agreement between theory and experiment, even for volume fractions up to 10%, a rather remarkable result.

In contrast, a survey of the available literature showed that very little data exist from well-controlled laboratory experiments for which deterministic multiple scattering effects could be studied. One exception we are aware of is the work by Bjørnø and Bjørnø [8], who used two stainless steel spheres in the laboratory to study the effects of sphere separation and angle of incidence on the backscattering of sound and compared the results with a simple model.

In this paper we derive a solution to a specific scattering problem using the multiple scattering expansion approach and compare it with experimental results. The experimental data consist of measurements of the pressure field backscattered from two nearly identical bubbles symmetrically placed the same distance  $d$  from the combined beam axis of the acoustic transmit and receive beams. The radius  $a$  of each bubble was  $(585 \pm 35) \mu\text{m}$ , with  $ka$  ranging from 0.2–0.35, where  $k$  is the acoustic wavenumber for the surrounding medium. The primary independent variable was  $d$ , and  $kd$  spanned the range from 0.2–21. In Sec. 1

the multiple scattering series is established and a closed form solution is derived, and in Sec. 2 the frequency response of a single bubble in water is reviewed. The experimental platform and the procedure are described in detail in Sec. 3, which includes the consideration of effects brought about by the geometry of the system. The experimental results are compared with the scattering model in Sec. 4, and found to be in good agreement, and a summary of the work is given in Sec. 5.

## 1 Multiple scattering theory

The simplest problem in multiple scattering is one involving just two identical, stationary scatterers symmetrically insonified by a plane wave at normal incidence. Intuition suggests that in such a case scattering will be completely coherent, since no randomness exists in the location of the scatterers or any other parameter. Various methods have been used to investigate this problem theoretically. For example, Twersky [13] obtained a closed form solution for two identical and isotropic scatterers insonified by single-frequency plane waves in terms of the scattering function of one of the scatterers. He went on to develop a set of equations that could be applied to problems involving arbitrary scatterers and angles of incidence. Twersky's work provides an intuitive description of the scattering process, one that can be extended to a variety of problems (for example see the work by Tolstoy [14], [15] on superresonant systems). Gaunard *et al.* [16] performed a partial summation of the multiple scattering series in terms of spherical harmonics and derived a pair of coupled equations that describe acoustic scattering by a pair of rigid and soft spheres for arbitrary angles of incidence. However, for the particular cases modeled the spheres were in the far field of each other, thereby mitigating strong multiple scattering effects. In this paper the multiple scattering series expansion will be used since for simple problems it is tractable and allows proper accounting of scattering terms of all orders.

The problem under consideration is the scattering of sound by a pair of bubbles (Fig. 1). A bistatic system is utilized to insonify the pair and receive the scattered pressure field in

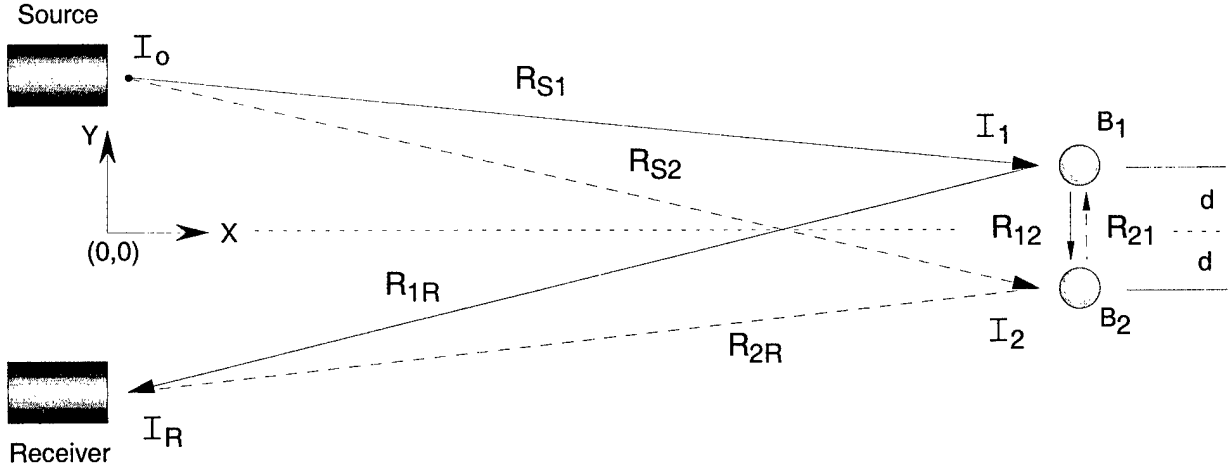


Figure 1: Geometry of the scattering problem (not to scale).

the frequency range 80 kHz to 140 kHz. The bubbles are of the same size, undeformed, and held fixed within the far field of the transducers. The speed of sound in the water is constant ( $c = 1490$  m/s), and the losses due to attenuation are negligible.

The complex pressure of the acoustic wave incident on bubble  $B_1$  due to the source can be written (dropping the  $e^{-i\omega t}$  term) as

$$p_{S1} = P_0 \frac{e^{ikR_{S1}}}{R_{S1}}, \quad (1)$$

and the pressure incident on bubble  $B_2$  as

$$p_{S2} = P_0 \frac{e^{ikR_{S2}}}{R_{S2}}. \quad (2)$$

Assuming that the pressure field scattered from each bubble propagates in the medium according to spherical spreading, even in the near field of the bubble (see Appendix A for justification of the assumption), the pressure of the acoustic field at the receiver due to bubble  $B_1$  becomes

$$p_{S1R} = p_{S1} f_{B1}(\theta_{SB_1R}, R_{1R}) \frac{e^{ikR_{1R}}}{R_{1R}}, \quad (3)$$

and that due to bubble  $B_2$  becomes

$$p_{S2R} = p_{S2} f_{B2}(\theta_{SB_2R}, R_{2R}) \frac{e^{ikR_{2R}}}{R_{2R}}. \quad (4)$$

In Eqs. (1), (2), (3), and (4)  $R_{S1}$  and  $R_{S2}$  are the distances from the source to bubbles  $B_1$  and  $B_2$ , respectively,  $R_{1R}$  and  $R_{2R}$  are the distances from the two bubbles to the receiver and  $f_{B_1}$  and  $f_{B_2}$  are the complex scattering functions of each bubble. The complex scattering function  $f_B(\theta, r)$  determines the amplitude and phase of the scattered wave at a distance  $r$  from the center of the bubble and angle  $\theta$  with respect to the incident plane wave. The scattering angles associated with the problem are shown in Fig. 2. The scattering function will be discussed in more detail in Sec. 2.

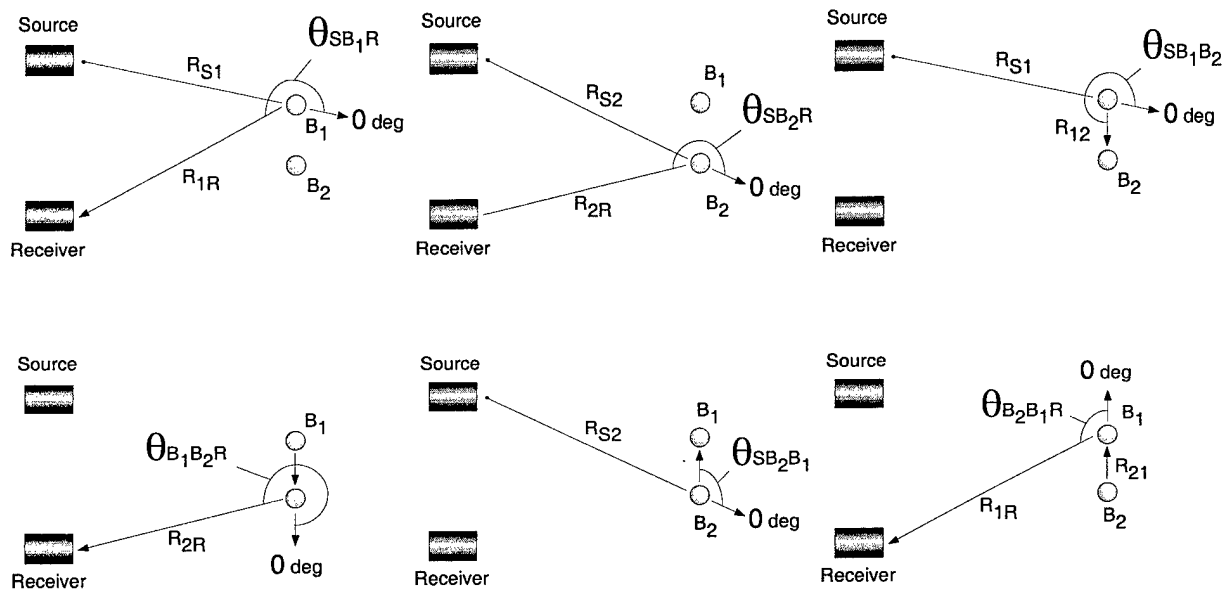


Figure 2: Scattering angles for the two bubble problem.

In the following we adopt a shorthand notation for the spherical spreading propagation terms, as  $\mathcal{P}_{\kappa\xi} = e^{ikR_{\kappa\xi}}/R_{\kappa\xi}$ , with  $R_{\kappa\xi}$  assuming the representation of the four distances noted above, namely,  $R_{S1}$ ,  $R_{S2}$ ,  $R_{1R}$  and  $R_{2R}$ . Looking ahead, the bubble-to-bubble distances  $R_{12}$  and  $R_{21}$  will also be used in subsequent calculations, with the corresponding propagation terms expressed as  $\mathcal{P}_{12}$  and  $\mathcal{P}_{21}$ . The distances between the various elements can be calculated with the aid of the position vectors constructed from the known geometry of the system. Substitution of Eqs. (1) and (2) into Eqs. (3) and (4) and summation of the latter

will give the complex pressure field at the receiver due to single scattering,

$$p_{SingleScatter} = P_0 [\mathcal{P}_{S1} f_{B1}(\theta_{SB_1R}, R_{1R}) \mathcal{P}_{1R} + \mathcal{P}_{S2} f_{B2}(\theta_{SB_2R}, R_{2R}) \mathcal{P}_{2R}]. \quad (5)$$

Note that for two stationary bubbles symmetrically arranged side by side, the intensity is the coherent one, and thus for two identical bubbles (i.e. the case studied herein), the scattering strength due to single scattering is  $20\log(2) = 6$  dB above the scattering strength of the single bubble.

In deriving the coherent intensity it is assumed that bubbles do not interact, an assumption that is violated when multiple scattering effects are induced owing to the proximity of the bubbles. To account for the interaction effects between the two bubbles, the multiple scattering series (MSS) will be developed. This will be accomplished with the help of the simplest graphical procedure of the *Feynman diagrams*, a method that was also used by Ye and Ding [11] to apply a correction to Foldy's theory. Adapted from Mattuck [17] (see pages 12-24) the MSS can be graphed as shown in Fig. 3, where each arrow represents a

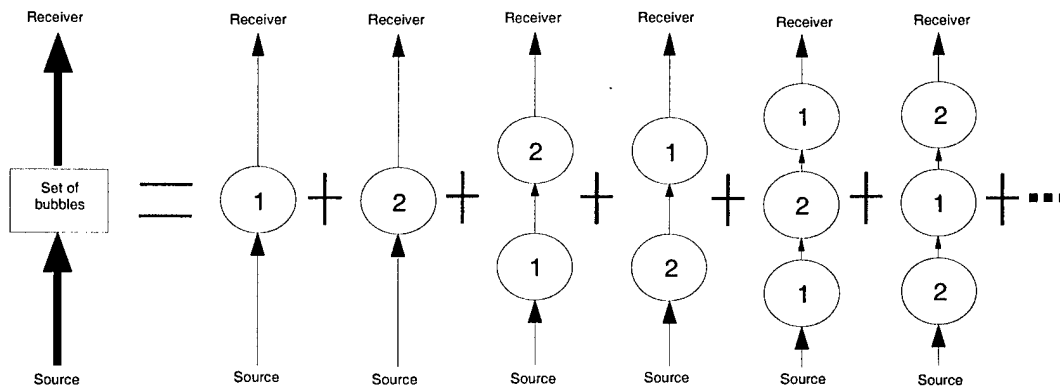


Figure 3: Diagram of the multiple scattering series for the two bubbles.

propagation term (describing spherical spreading) and each circle represents scattering from a bubble. The two single scattering events described by Eqs. (3) and (4) are shown as the first two terms of the series. The third and fourth terms represent the one-way scattering events and are written as

$$p_{S12R} = p_{S1} f_{B1}(\theta_{SB_1B_2}, R_{12}) \mathcal{P}_{12} f_{B2}(\theta_{B_1B_2R}, R_{2R}) \mathcal{P}_{2R}, \quad (6)$$

and

$$p_{S21R} = p_{S2}f_{B2}(\theta_{SB_2B_1}, R_{21})\mathcal{P}_{21}f_{B1}(\theta_{B_2B_1R}, R_{1R})\mathcal{P}_{1R}. \quad (7)$$

The fifth and sixth terms in the MSS represent the double scattering events, which are expressed as

$$p_{S121R} = p_{S1}f_{B1}(\theta_{SB_1B_2}, R_{12})\mathcal{P}_{12}f_{B2}(180^\circ, R_{21})\mathcal{P}_{21}f_{B1}(\theta_{B_2B_1R}, R_{1R})\mathcal{P}_{1R}, \quad (8)$$

and

$$p_{S212R} = p_{S2}f_{B2}(\theta_{SB_2B_1}, R_{21})\mathcal{P}_{21}f_{B1}(180^\circ, R_{12})\mathcal{P}_{12}f_{B2}(\theta_{B_1B_2R}, R_{2R})\mathcal{P}_{2R}. \quad (9)$$

For brevity, we let

$$\mathcal{Z} = \mathcal{P}_{21}f_{B1}(180^\circ, R_{12})\mathcal{P}_{12}f_{B2}(180^\circ, R_{21}). \quad (10)$$

Higher order terms in the MSS can be written simply by multiplying Eqs. (6), (7), (8) and (9) by an appropriate power of  $\mathcal{Z}$ . For example, the triple scattering terms can be written as

$$p_{S1212R} = p_{S12R} \cdot \mathcal{Z}^1 \quad \text{and} \quad p_{S2121R} = p_{S21R} \cdot \mathcal{Z}^1. \quad (11)$$

Summing all terms of the MSS results in the total pressure at the receiver,  $p_T$ , which can be written as

$$p_T = P_0 \cdot \sum_{\kappa=1}^2 \sum_{\xi=1}^2 \mathcal{P}_{S\kappa}f_{B\kappa}(\theta_{SB_\kappa R}, R_{\kappa R})\mathcal{P}_{\kappa R} + \left[ \mathcal{P}_{S\kappa}f_{B\kappa}(\theta_{SB_\kappa B_\xi}, R_{\kappa\xi})\mathcal{P}_{\kappa\xi}f_{B\xi}(\theta_{\kappa\xi R}, R_{\xi R})\mathcal{P}_{\xi R} + \mathcal{P}_{S\kappa}f_{B\kappa}(\theta_{SB_\kappa B_\xi}, R_{\kappa\xi})\mathcal{P}_{\kappa\xi}f_{B\xi}(180^\circ, R_{\xi\kappa})\mathcal{P}_{\xi\kappa}f_{B\kappa}(\theta_{B_\xi B_\kappa R}, R_{\kappa R})\mathcal{P}_{\kappa R} \right] \times \frac{1}{1 - \mathcal{Z}}, \quad (12)$$

where,  $\kappa \neq \xi$ .

In Eq. (12) the term  $1/(1 - \mathcal{Z})$  arises from the fact that the higher order terms that multiply the term in brackets form the series  $(1 + \mathcal{Z} + \mathcal{Z}^2 + \dots)$ , which is geometric. For a similar problem the generalized closed form solution obtained by Twersky [13] is  $2\mathcal{H}(r) \cos(kd \sin \theta)A/[1 - A\mathcal{H}(2d)]$  where  $A$  is the complex scattering function of a monopole,  $r$  is the distance from the bubbles to the receiver,  $\mathcal{H}(r)$  describes the propagation from the

bubbles to the receiver,  $\mathcal{H}(2d)$  is the bubble to bubble propagation term and  $\theta$  is the relative bearing of the receiver from the pair of bubbles (see Sec. 1.2 in [13]). Note that for our specific case of backscattering  $\theta = 180$  degrees, and  $\mathcal{H}(r) = e^{ikr}/r$ .

Our Eq. (12) is an exact solution for the any two-bubble problem, insofar as the bubble scattering function need not assume a purely monopole form. The bubbles can be of different size while the geometry of the problem can be arbitrary. Provided the scattering function of each bubble is known, and the propagation terms can be determined from the geometry of the system, the response of the pair of bubbles can be determined. Equation (12) will be used in Sec. 4 to model the experiment. Importantly, our solution reduces to Twersky's concise expression for the case of scattering from two identical monopoles.

## 2 The response of a single gas bubble in water

The general solution for scattering from a fluid sphere was derived by Anderson [18], who found that the scattered pressure field equals

$$p_B = -p_{inc} \sum_{m=0}^{\infty} A_m P_m(\cos \theta) h_m^{(1)}(kr). \quad (13)$$

In Eq. (13)  $p_{inc}$  is the pressure field of the wave incident on the sphere,  $P_m$  is the Legendre polynomial of order  $m$ ,  $\theta$  is the scattering angle,  $h_m^{(1)}$  is the order  $m$  spherical Hankel function of the first kind,  $k$  is the wavenumber of the surrounding medium,  $r$  is the range from the sphere to a point in the field, and the amplitude coefficient  $A_m$  is given by

$$A_m = \frac{(-i)^m (2m+1)}{1 + iC_m}. \quad (14)$$

For a bubble of radius  $a$  filled with gas of density  $\rho_b$  and speed of sound  $c_b$  immersed in a fluid with density  $\rho_f$  and speed of sound  $c_f$  the coefficient  $C_m$  equals

$$C_m = \frac{\frac{mj_{m-1}(k_b a) - (m+1)j_{m+1}(k_b a) n_m(ka)}{mj_{m-1}(ka) - (m+1)j_{m+1}(ka)} \frac{mj_{m-1}(ka) - (m+1)j_{m+1}(ka) \rho_b c_b}{mj_{m-1}(ka) - (m+1)j_{m+1}(ka) \rho_f c_f}}{\frac{mj_{m-1}(k_b a) - (m+1)j_{m+1}(k_b a) j_m(ka)}{mj_{m-1}(ka) - (m+1)j_{m+1}(ka)} \frac{\rho_b c_b}{\rho_f c_f}}, \quad (15)$$

where  $j_m$  is the spherical Bessel function,  $n_m$  is the spherical Neumann function and  $k_b$  is the wavenumber for the gas in the bubble.

We remark that for bubbles very small compared to the wavelength of the sound ( $ka \ll 1$ ), the solution can be simplified significantly. In this case, the complex scattering function can be written as

$$f_B|_{ka \ll 1} = \frac{a}{\left(\frac{f_{\text{res}}}{f}\right)^2 - 1 - i\delta} \quad (16)$$

where  $f$  is the insonifying frequency,  $\delta$  is the total damping coefficient (see Devin [19]), and  $f_{\text{res}}$  is the resonant frequency of the bubble. Note that Eq. (16) is consistent with the  $e^{-i\omega t}$  dependence. When insonified at the resonance frequency  $f = f_{\text{res}}$ , the amplitude of the bubble wall oscillation is maximized, producing the well defined peak in the frequency response curve (see Fig. 5a). For an air bubble located at depth  $z$  meters in water the resonant frequency can be approximated as

$$f_{\text{res}} = \frac{3.25\sqrt{1 + 0.1z}}{a}, \quad (17)$$

where for  $a$  expressed in meters the resonant frequency is obtained in hertz. Note that Eq. (16) is independent of the scattering angle. Derivations and additional comments can be found in standard texts (e.g., Ref. [20]). For the present case, the variable  $ka$  ranges from 0.2 to 0.35, which is not sufficiently small to allow the use of Eq. (16), and thus we use Eq. (13) to calculate the response of the bubble. The primary reason is that the insonified bubble oscillates back and forth in response to the forcing of the acoustic wave. The oscillation of the bubble will be out of phase with the oscillation of the surrounding medium, owing to the difference in density, giving rise to a weak dipole term. Consequently, an additional term, provided by Eq. (13), is needed to describe of the pressure field scattered by the bubble. Finally, we remark that the general solution only accounts for radiation damping and neither viscous nor thermal damping. However, this does not introduce any errors in our calculations because for frequencies much higher than the resonant one, the total damping is not affected by the viscous and thermal components. Further comments on the differences between the general solution and the low  $ka$  approximation are presented in Sec. 4.

Utilizing Eq. (13), the complex scattering function of the bubble is thus given by

$$f_B(\theta, r) = -\frac{r}{e^{ikr}} \sum_{m=0}^1 A_m P_m(\cos \theta) h_m^{(1)}(kr), \quad (18)$$

and should not be confused with the far field form function [21], which is a dimensionless representation of the scattered field and is independent of  $r$ . Equation (18) represents only two modes; the first ( $m = 0$ ) describes the monopole radiation (breathing mode) of the bubble (thus is analogous to Eq. (16) with differences pertaining to aforementioned damping), while the second ( $m = 1$ ) describes the dipole radiation. Higher order modes are suppressed in the calculations because they have negligible effect in the  $ka$  range of interest. For example, if the longitudinal quadrupole mode ( $m = 2$ ) is included in Eq. (18), then, for a  $585 \mu\text{m}$  bubble insonified by an 140 kHz acoustic wave, the magnitude difference in the backscattering direction is

$$20 \log \left( \frac{|f_B|_{m=0,1,2}}{|f_B|_{m=0,1}} \right) = 0.014 \text{ dB}. \quad (19)$$

The Legendre polynomial of order zero,  $P_0(\cos \theta)$ , equals 1, while the polynomial  $P_1(\cos \theta)$  equals  $\cos \theta$  (see [22] page 333), giving

$$f_B(\theta, r) = -\frac{r}{e^{ikr}} \left[ A_0 h_0^{(1)}(kr) + A_1 \cos \theta h_1^{(1)}(kr) \right], \quad (20)$$

which will be combined with Eq. (12) to model the experiment.

Numerical results for backscattering from both single bubbles and the pair of bubbles will be reported in terms of target strength (TS). For single bubbles, the square of the magnitude of  $f_B$  evaluated in the backscattered direction ( $\theta = 180^\circ$ ) gives the backscattering cross section,  $\sigma_{bs}$ , with TS given by

$$\text{TS} = 10 \log \sigma_{bs}, \quad (21)$$

in dB re  $1 \text{ m}^2$ . For the pair of bubbles, the total scattered pressure at the receiver  $p_T$ , given by Eq. (12), is related to TS using

$$\text{TS} = 10 \log \left( \frac{|p_T|^2}{|p_{inc}|^2} \cdot R_{BR}^2 \right), \quad (22)$$

where  $p_{inc}$  is the incident pressure at the bubbles and  $R_{BR}$  is the distance from the bubbles to the receiver. For an exact calculation of the TS, the pressure  $p_{inc}$  should be substituted by  $p_{S1}$  and  $p_{S2}$  (Eqs. (1) and (2)), while the  $R_{BR}$  should be replaced by the distances  $R_{1R}$  and  $R_{2R}$ .

### 3 Experimental apparatus and procedure

The experiments were performed in a plexiglass tank of dimensions  $1.2 \text{ m} \times 0.45 \text{ m} \times 0.51 \text{ m}$  ( $L \times W \times H$ ) filled with fresh water to a height of 45 cm. Its bottom, front, and back walls were lined with anechoic material to reduce reflections, and all the surfaces of the tank were thoroughly wetted. The two immersion transducers were arranged in a bistatic configuration. The transducers were Panametrics model V1011, with a peak frequency of 104 kHz and minus 6 dB points at 70 kHz and 140 kHz. All the experiments were performed at a frequency range of 80 kHz to 140 kHz, henceforth referred to as “operational frequency

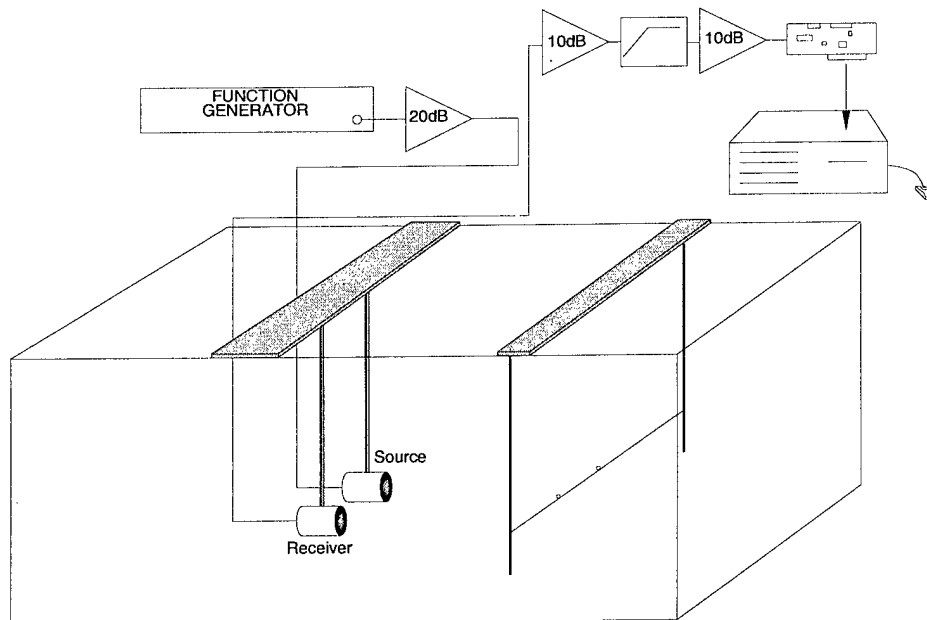


Figure 4: Experimental apparatus.

range". The transducers were inserted in closed-cell Neoprene tubes to reduce the effect of reflections from the sides of the tank. The source was driven in a pulse mode using a six-cycle tone burst at a very low duty cycle, enabling resolution of the bubble signal. A computer equipped with a data acquisition card (1 MHz sampling rate) and data acquisition software acquired the amplified signal. A schematic of the apparatus is shown in Fig. 4. For each measurement, 20 waveforms were averaged and band-pass filtered, and the root-mean-squared voltage of the signal was calculated and squared.

The system was calibrated using an 18.2 mm radius tungsten-carbide sphere as a reference target. The theoretical analysis of the response of the tungsten-carbide sphere to continuous waves was based on the work by Faran [23] corrected according to a comment by Hickling [24]. The inherent bandwidth associated with a finite pulse was accounted for using a procedure described by Foote [25].

A fine waxed nylon thread (approximately 150  $\mu\text{m}$  in diameter) held the bubbles in place by virtue of the bubbles adhering to it. Leighton *et al.* [26] studied the resonant-frequency properties of millimeter-sized bubbles also by using a wire to which free floating bubbles adhered. In their case, the wire alone produced a measurable response, which was subtracted from the combined bubble-and-wire response, and good agreement was achieved between optical and acoustic sizing. In our work, the thread alone did not return a signal above the noise floor, which was approximately 20 dB below the level of the signal from the single bubble target.

The thread was attached to a thin wire frame and positioned on the axis of the combined beam, at a depth of 18 cm. The distance from the transducers to the thread was  $R_0 = 0.58$  m, which puts the targets well into the far field. The Rayleigh distance was 0.5 m at 140 kHz (see below for explanation). The absorption coefficient for fresh water at 100 kHz is about 0.005 dB/m [27] at the tank temperature of 20°C, which for the roundtrip distance of 1.6 m makes attenuation negligible.

Bubbles were created using a 26 gauge hypodermic needle. Since the rate of release of the bubbles was pressure controlled, there was some variation in the size of the bubbles created,

an effect that has been investigated by others [28], [29]. However, with practice we could produce same-sized bubbles with good consistency. The size of the bubbles was measured with the acoustic system and found to be  $(585 \pm 35) \mu\text{m}$  (see Fig. 5). The size was determined by comparing the TS of a single bubble measured across the operational frequency range with the equivalent best-fit frequency-response curve obtained by Eq. (18), expressed in TS according to Eq. (21). Since the response is flat in the operational frequency range, the bandwidth of the six-cycle tone burst has no effect in the calculated response which pertains to CW excitation. The size was also checked independently using optical means. In that

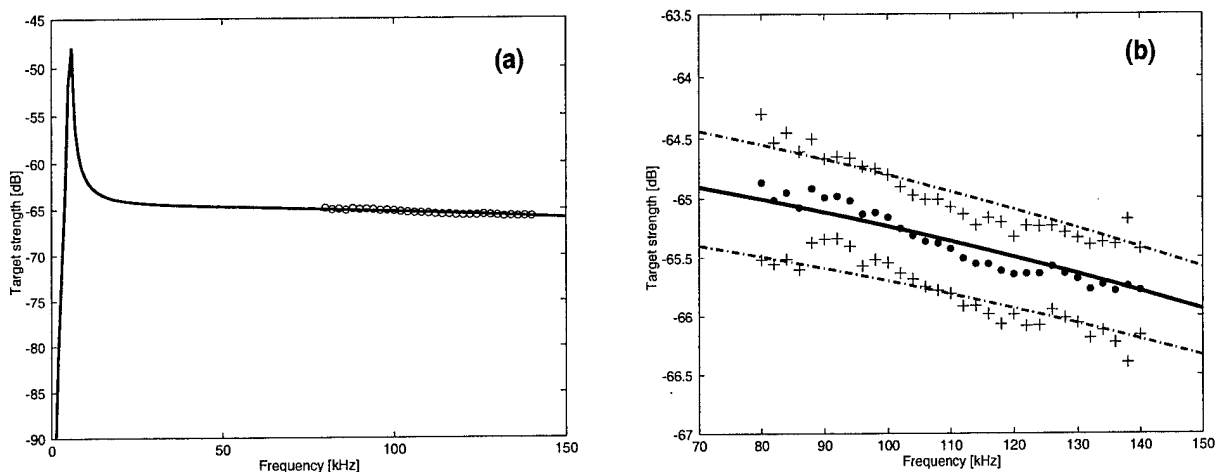


Figure 5: Frequency response of a single bubble of radius  $585 \mu\text{m}$ , theory vs data. Graph (b) is a detail of graph (a). The middle line is the theoretical response of the  $585 \mu\text{m}$  bubble, while the upper line is for a  $620 \mu\text{m}$  bubble and the lower line for a  $550 \mu\text{m}$  bubble. The dots and crosses are the means and standard deviations of 18 experiments.

case a piece of thread was glued on a Petri dish and placed under a microscope, and the same procedure was used to produce and place bubbles on the thread as the one used in the actual experiments. The optically determined size was  $(575 \pm 40) \mu\text{m}$ . This includes the required correction in the size due to the hydrostatic pressure at a depth of 18 cm. The optical system also verified that there was no significant change in the shape of the bubbles (see Fig. 6).

After the bubbles were created, they rose toward the surface and adhered to a thin metal rod. The bubbles, with the aid of the rod, were in turn placed at a predetermined spot on the thread a distance  $d$  from the combined beam axis of the set of transducers.

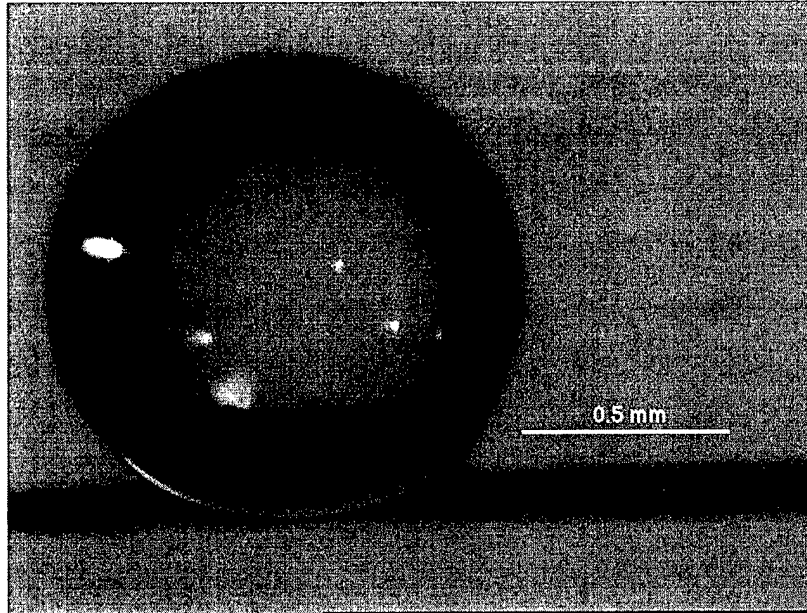


Figure 6: Single bubble on the fine thread. The radius of bubble is  $(585 \pm 35) \mu\text{m}$ . Note that there is no significant distortion of the shape.

As soon as the set of bubbles was placed in position, the TS was measured from 80 kHz to 140 kHz in increments of 2 kHz. When the experiment was completed, a new set of bubbles replaced the old one. Each experiment required  $\approx 10$  minutes. Reduction of the TS due to dissolution of the gas during that time was minimal (about 0.1 dB).

Bubble separation was parameterized using the variable  $kd$ , where  $d$  is the distance from the center of each bubble to the axis of the combined beam. Because of the limited frequency range, it was necessary to perform the experiments for several distances  $d$  in order to span a larger  $kd$  range. The minus 3 dB two-way half-angle,  $\phi_{3dB}/2$ , at 140 kHz was  $3.8^\circ$ , which at  $R_0 = 0.58$  m reduced the maximum usable  $d$  to 38 mm. Note that this is well within the radius of the first Fresnel zone, equal to about 55 mm at 140 kHz. Thus, experimental data

were acquired for  $d$  equal to 0.6, 1.5, 2, 2.5, 3, 5, 10, 15, 20, 25, 30, and 35 mm, and thus the variable  $kd$  ranged from 0.2 to 21. The distance  $d$  was measured with an uncertainty of  $\pm 0.5$  mm. At least four experiments were performed at each position to average out the experimental errors associated with the variable size of the bubbles and their positioning on the thread. The mean of the measurements is used in Sec. 4 for comparison with the model.

Finally, two effects brought about by the geometry of the system need to be considered. These effects are the directivity pattern of the set of transducers and the directivity pattern of the pair of bubbles. The directivity pattern of the transducers reduces the signal level of targets that are off the axis of the beam. Therefore, it was necessary to correct the data accordingly (since one of the assumptions in the theory was that the targets are on the axis of the beam). It is convenient to obtain the two-way beam pattern of the set of transducers and model it as the beam of a single transducer of some equivalent diameter. Accordingly, transverse profiles of the beam at  $R_0 = 0.58$  m, at various frequencies, were obtained using a standard target (the tungsten-carbide sphere), and a Gaussian beam profile was fitted to the data. Over the operational frequency range, the measured minus 3 dB beamwidth of the two-way beam,  $\phi_{3dB}$  expressed in degrees, was used to infer an equivalent aperture diameter using  $\phi_{3dB} \approx 59(\lambda/D)$ , giving  $D \approx 83$  mm. Thus the Rayleigh distance of the transducer pair, defined as  $R_d = \pi D^2/(4\lambda)$ , is  $R_d = 0.5$  m for our highest frequency of 140 kHz. With the beam pattern (out to the minus 3 dB level) completely characterized, the correction of the data became feasible.

In addition, since each insonified bubble intercepts and scatters sound, an assemblage of them will behave like an array of sources, and two bubbles in line will behave like a two-element line array. The directivity pattern of the far-field radiation pressure of a two-element broadside line array is [30]

$$H(d, f, \theta) = |e^{-ikd \sin \theta} (1 + e^{ik(2d) \sin \theta})| \quad (23)$$

where  $d$  is the distance from the center of a bubble to the axis of the combined beam,  $f$  is the insonifying frequency, and  $\theta$  is the scattering angle. When the two bubbles are side by side the pattern is almost omnidirectional; as  $2d$  increases the main lobe of the array

becomes narrower and multiple side lobes appear. This effect was verified experimentally. A hydrophone mounted on a translation stage was used to obtain transverse beam profiles 30 cm from the bubbles. Figure 7 compares the theory and the experimental data.

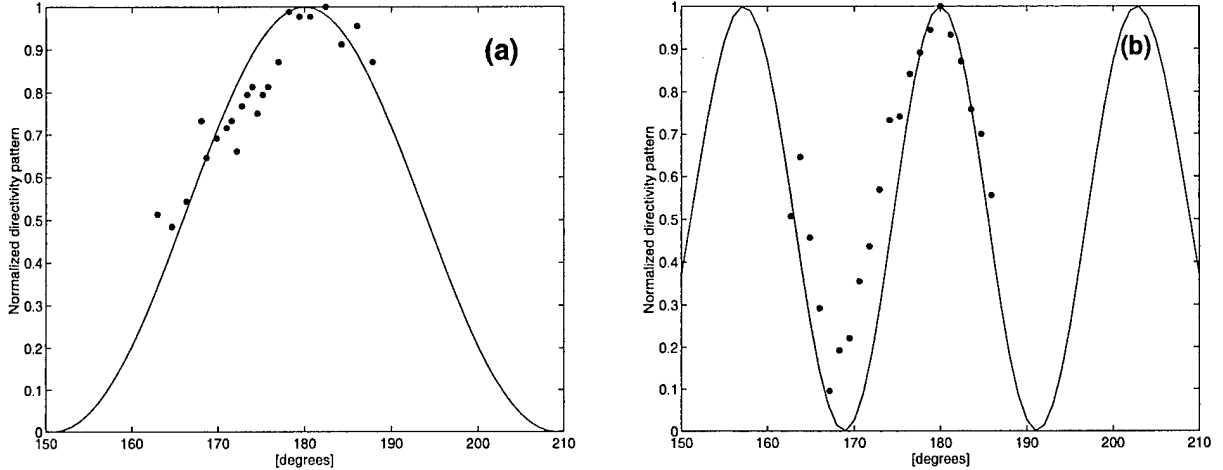


Figure 7: Theoretical directivity pattern for a two-element line array (solid curve) vs experimental data (dots). Graph (a) shows the pattern for  $2d = 11$  mm and  $f = 140$  kHz. Graph (b) is for  $2d = 31$  mm and  $f = 125$  kHz.

## 4 Results and interpretation

Considering that the monostatic configuration is a common geometry for many practical applications, we decided to co-locate the source and receiver in the model, thus placing both transducers at position  $(x = 0, y = 0)$  (see Fig. 1), and correct the experimental data utilizing the predetermined directivity patterns of the transducers and the bubbles. The constants used in all of the simulations were: (a) speed of sound  $c = 1490$  m/s; (b) mean bubble radius  $a = 585$   $\mu\text{m}$ ; (c) distance from transducers to set of bubbles  $R_o = 0.58$  m; (d) depth of bubbles  $z = 0.18$  m. Based on the known geometry of the system, the propagation terms were established and, with the incorporation of Eqs. (18) and (22), the TS at the receiver was calculated. Figure 8 shows the theoretical curve for backscattering at 110 kHz

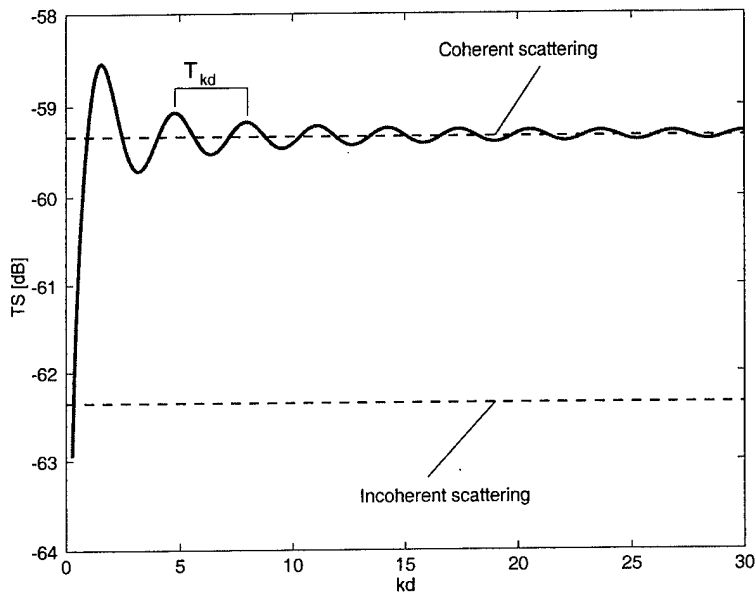


Figure 8: Theoretical curve for backscattering from two  $585 \mu\text{m}$  bubbles at a frequency of 110 kHz and variable  $d$ , which is the distance from the combined beam axis to the center of each bubble.

versus  $kd$ , with straight lines representing the coherent and incoherent scattering from two identical bubbles. The oscillatory behavior is brought about by the interference of the waves scattered between the bubbles. For the specific case shown in Fig. 8 the first maximum occurs at  $kd \approx 1.6$ , with successive maxima occurring every  $T_{kd} \approx 3.2$ . This implies that constructive interference results for

$$2d|_{\max,\alpha} \approx (2\alpha + 1)\frac{\lambda}{2} \quad (\alpha = 0, 1, 2, 3, \dots), \quad (24)$$

while destructive interference results for

$$2d|_{\min,\alpha} \approx \alpha\lambda. \quad (25)$$

Note that the amplitude of the oscillation diminishes with increasing  $kd$ ; for  $kd \rightarrow \infty$  the curve asymptotes to the exact coherent backscattering level. (Simulations showed that Eqs. (24) and (25) hold true across the operational frequency range).

In Figs. 9a and 9b several theoretical curves (solid lines) for backscattering at fixed frequencies and variable  $d$  are compared with experimental data (dots). The black line represents backscattering from two 585  $\mu\text{m}$  bubbles, this radius being our best estimate of the mean size of each bubble. The two gray lines represent calculations pertaining to two bubbles each of radius 620  $\mu\text{m}$  (upper line) and 550  $\mu\text{m}$  bubbles (lower line). As mentioned in Sec. 3, 35  $\mu\text{m}$  is our best estimate of the standard deviation of the expected bubble radius; thus, these curves represent bounds to the experimental results.

The scattering calculations were carried out for fixed frequency (as shown in Figs. 9a and 9b) and variable  $d$ . The calculated pressure was then expressed in terms of target strength and plotted against the parameter  $kd$ . The data are the ensemble average of the multiple experiments at each position. For clarity, the standard deviation of each measurement is not shown. It varied between  $\pm 0.2$  dB to  $\pm 1$  dB, depending on the proximity of the bubble signal to the noise floor (explained below). To compare the data with the simulations, the corrections mentioned in Sec. 3 were applied to the data. More specifically, the fitted Gaussian beams (over the operational frequency range) were used to calculate the loss (in dB) due to the bubbles being off axis of the combined beam of the transducers,

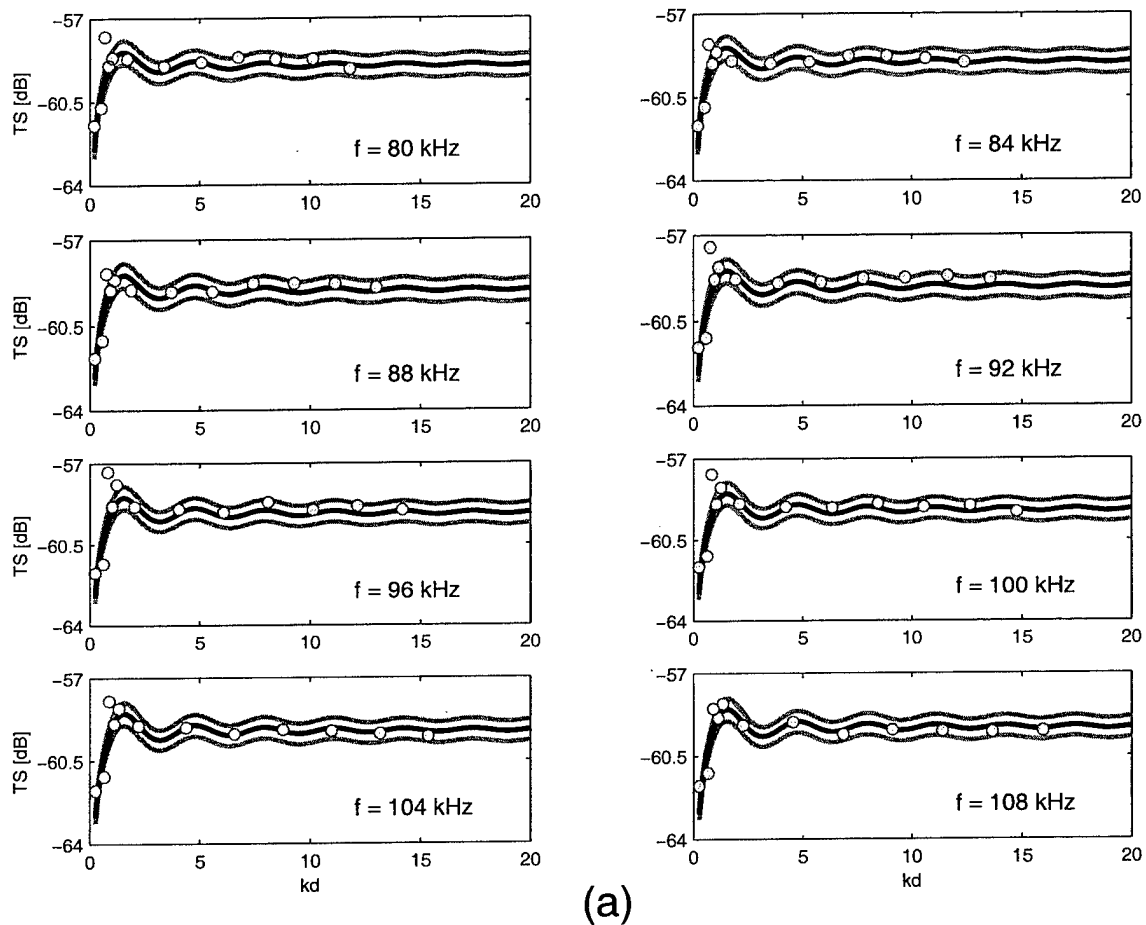


Figure 9a: Theoretical curves for backscattering from two bubbles of radius  $(585 \pm 35) \mu\text{m}$  for fixed frequency (as shown) and variable  $d$  versus experimental data (dots). The black line represents backscattering from two  $585 \mu\text{m}$  bubbles. The data are bounded by the responses of two  $620 \mu\text{m}$  bubbles (upper gray line) and two  $550 \mu\text{m}$  bubbles (lower gray line).

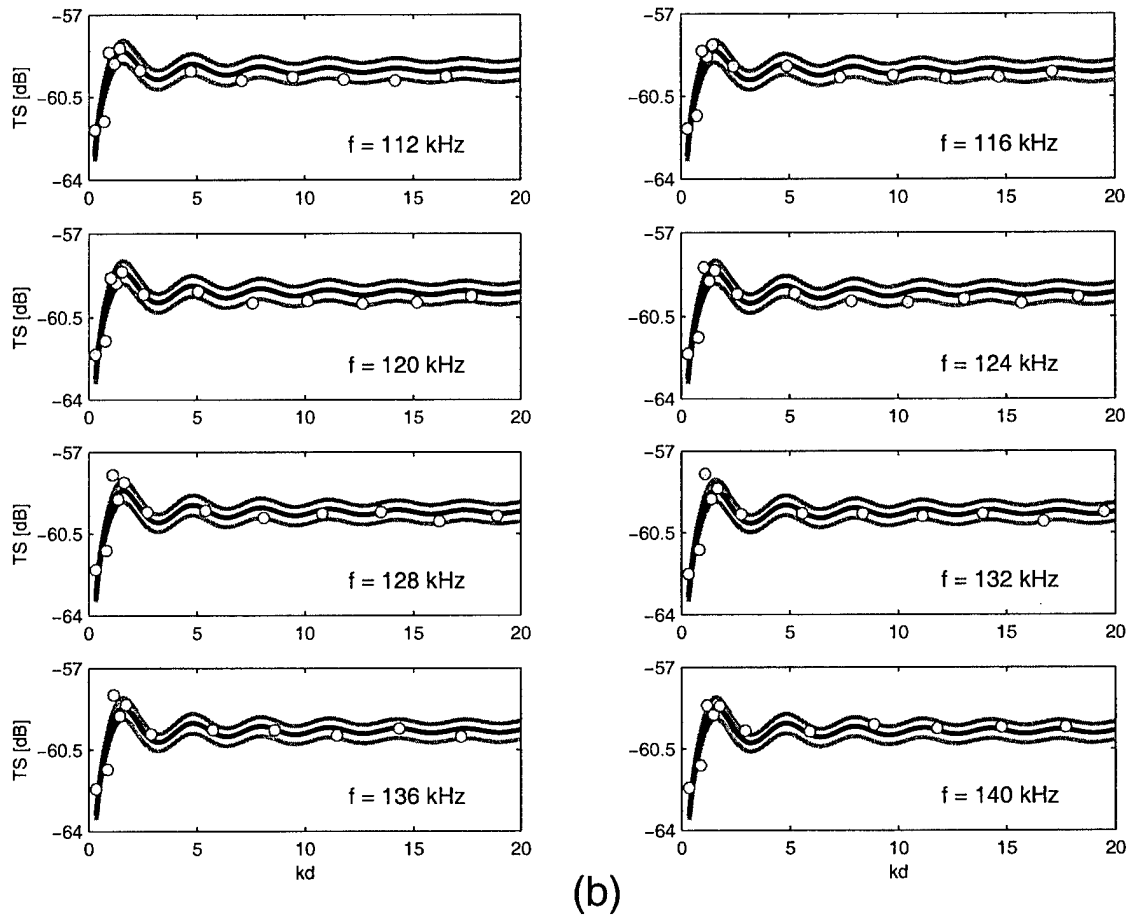


Figure 9b: Theoretical curves for backscattering from two bubbles of radius  $(585 \pm 35) \mu\text{m}$  for fixed frequency (as shown) and variable  $d$  versus experimental data (dots). The black line represents backscattering from two  $585 \mu\text{m}$  bubbles. The data are bounded by the responses of two  $620 \mu\text{m}$  bubbles (upper gray line) and two  $550 \mu\text{m}$  bubbles (lower gray line).

while Eq. (23) was used to determine the loss (in dB) of the pressure at the receiver due to the pattern of the two-bubble array. The losses calculated were added to the measured TS to approximate the monostatic configuration for which the bubbles are on the axis of the combined beam.

In Figs. 9a and 9b the theoretical curves model the response to CW excitation. However, data was acquired using a six-cycle tone burst, which reduces the effects of multiple scattering as the distance between the two bubbles increases. To see how the tone burst influences the maximum  $kd$  that includes multiple scattering effects, we let  $t_{on}$  be the on time of the tone burst and  $t_T$  be the time it takes sound to travel from one bubble to the neighbouring one. Then, we can write

$$\frac{t_{on}}{t_T} = \frac{\pi \cdot \text{cycles}}{kd}, \quad (26)$$

where, the variable *cycles* represents the number of cycles in the tone burst. Considering that the length of the pulse should be at least two times  $2d$  to observe multiple scattering effects, we deduce that  $kd < 9$ , for a six-cycle tone burst. For higher  $kd$  the absence of significant interaction between the bubble will result in coherent scattering, equal to the TS of a single bubble plus  $20 \log(2)$ .

The experimental data agree reasonably well with the response predicted by the model. For  $kd > 9$  the backscatter can be modeled as purely coherent, since the interaction effects are negligible and the scatter resembles single scattering. The increased scatter of the experimental data for  $kd > 7$  is due to beam width and directivity of the two-bubble array. As the separation between the bubbles increased, they fell off the axis of the combined beam of the transducers and, at the same time, the main lobe of the two-bubble array became narrower. Therefore, the signal received became weaker with increasing bubble separation, and the TS approached the noise floor (which was equivalent to a scatterer with TS equal to -80 dB, while located on-axis of the beam).

For  $kd < 1.6$  the backscattered radiation level is reduced considerably, presumably due to the effect of the mutual radiation impedance. The pressure radiated from one bubble applies a force to the neighboring one, altering in the process its radiation impedance, which becomes

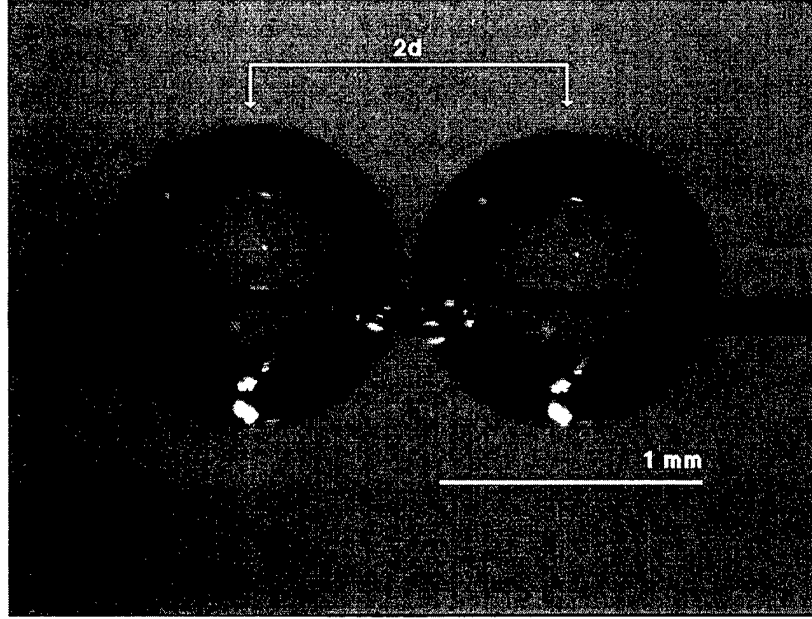


Figure 10: Photograph of two bubbles separated by center-to-center distance  $2d \approx 1.2$  mm, equivalent to  $kd \approx 0.2$  at 80 kHz.

a sum of the self and mutual radiation impedances. As  $kd \rightarrow 0$  reactance dominates, and the velocity of the fluid particles are out of phase with the pressure and therefore reradiation is less efficient. Note that this is very similar to the problem of interactions between closely packed elements of arrays [31], [32]. Interestingly, when  $kd$  falls below 0.3, the TS approaches that of a  $740 \mu\text{m}$  bubble, i.e. a bubble with a volume equal to twice the volume of a  $585 \mu\text{m}$  bubble. At  $kd \approx 1.6$  the individual waves scattered from the bubbles add in phase, while the bubbles are not sufficiently far from each other that the dipole term is unimportant. The combination of the increased magnitude and the constructive addition of the phases of the waves results in excess radiation. Note that the transition from reduced scatter to excess scatter to coherent scatter occurs very rapidly.

Finally, it should be mentioned that the incorporation of the complex scattering function for  $ka \ll 1$  in the model (or in Twersky's concise expression mentioned in Sec. 1) produced similar results with less computational strain. However, there were two differences that

necessitated the use of the general solution. First, the magnitude of the frequency response for a single bubble calculated with the low  $ka$  approximation results in increased backscatter levels, since  $ka$  is nominally 0.3 for our case. For example, at 140 kHz the TS calculated using Eq. (16) is about 0.65 dB higher than the TS calculated using Eq. (18), an error that carries over in the outcome of Eq. (12). Second, the amplitude of the oscillation (e.g. that seen in Fig. 8), when calculated using the multimodal scattering function in Eq. (12) is slightly higher than this amplitude when calculated using the simplified scattering function. The reason is that the amplitudes of the scattered waves, which depend on scattering angle and distance from the bubble, are correctly accounted for, by the combination of Eqs. (18) and (12). Admittedly, these differences are subtle for the geometry studied here (i.e., monostatic configuration and symmetrically arranged bubbles normal to the incident wave). However, we emphasize that our modeling approach is a general one that can be used with almost no modifications for bubbles with high  $ka$ , arbitrary sizes, and scattering geometries. This will be exploited in future work.

## 5 Summary

The problem of backscattering of sound from two bubbles was studied theoretically and experimentally in the frequency range 80–140 kHz. An exact, closed-form solution, based on the expansion of the multiple scattering series, was derived and used to model the backscattering response of the two bubble system. Well-controlled experiments were performed by insonifying two identical bubbles attached to a fine thread, at an angle of  $90^\circ$  with respect to the two-bubble axis. The radius  $a$  of each bubble was  $585 \mu\text{m}$ , which translates to a  $ka$  range of 0.2–0.35, where  $k$  is the wavenumber of the medium. By varying the separation distance  $d$  between each bubble and the axis of the two-way beam, we spanned the range of  $kd$  from 0.2–21. The thread did not register a signal above the noise floor; furthermore, measurement of the size of single bubbles showed that it did not interfere with the response of the bubbles. Comparison of the numerical model and the experimental data showed good

agreement. The constructive and destructive interference of the multiply scattered waves induces an oscillation about the exact coherent scattering level, with diminishing amplitude for increasing separation. At  $kd \approx 1.6$  ( $2d \approx \lambda/2$ ) the backscattered radiation was maximized, while for  $kd < 1.6$  ( $2d < \lambda/2$ ) interference effects resulted in reduced pressure levels.

## Acknowledgments

The authors wish to thank Dr. Steven Kargl of the Applied Physics Laboratory for the loan of certain instrumentation and for providing valuable feedback. We also appreciate the insightful comments from an anonymous reviewer. This work was funded by the Office of Naval Research, Code 321 OA.

## A Appendix

In Sec. 2 the pressure field scattered by a bubble was written as

$$p_B = -p_{inc} \sum_{m=0}^{\infty} A_m P_m(\cos \theta) h_m^{(1)}(kr). \quad (\text{A1})$$

It was established that in the  $ka$  range 0.2–0.35 only the modes zero and one are significant, therefore, Eq. (A1) (normalized) can be written as

$$\frac{p_B}{p_{inc}} = - \left[ A_0 h_0^{(1)}(kr) + A_1 \cos \theta h_1^{(1)}(kr) \right]. \quad (\text{A2})$$

The spherical Hankel functions of order zero and one can be expressed in terms of the free-field Green's function as

$$h_0^{(1)}(kr) = -\frac{i}{k} \frac{e^{ikr}}{r}, \quad (\text{A3})$$

and

$$h_1^{(1)}(kr) = -\frac{i}{k} \frac{e^{ikr}}{r} \left( \frac{1}{i} + \frac{1}{kr} \right). \quad (\text{A4})$$

By substitution of Eqs. (A3) and (A4) in Eq. (A2), the normalized scattered pressure field becomes

$$\frac{p_B}{p_{inc}} = \frac{i}{k} \frac{e^{ikr}}{r} \left[ A_0 + A_1 \cos \theta \left( \frac{1}{i} + \frac{1}{kr} \right) \right]. \quad (\text{A5})$$

Study of Eq. (A5) reveals that in the far field the monopole term is clearly dominant. For example, for backscattering at 140 kHz

$$20 \log \left( \frac{|A_0 h_0^{(1)}(kr)|}{|A_1 \cos \theta h_1^{(1)}(kr)|} \right) \approx 20 \log \left( \frac{|A_0|}{|-A_1(-i)|} \right) = 18.95 \text{ dB}. \quad (\text{A6})$$

In the near field the weak dipole term becomes important, but the breathing mode of the bubble remains responsible for most of the energy reradiation. Therefore, propagation of the scattered pressure approximates spherical spreading. In Fig. 11 we graph Eq. (A5)

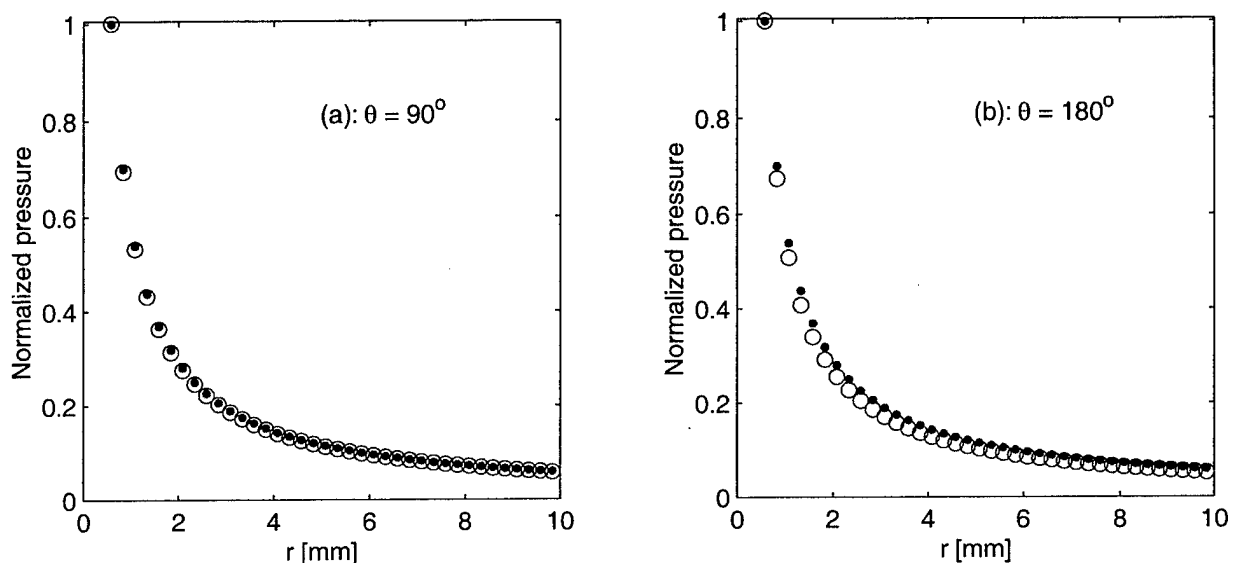


Figure 11: Comparison between Eq. (A5) (circles) and the normalized spherical spreading approximation  $1/r$  (dots).

(circles) against the normalized spherical spreading approximation  $1/r$  (dots) for two cases: (a)  $\theta = 90^\circ$  and (b)  $\theta = 180^\circ$ .

In the first case, the dipole term has no effect, since  $\cos 90^\circ = 0$ , therefore the agreement between the actual pressure reduction and spherical spreading is practically perfect. In the second case, the dipole term has maximum effect, since  $\cos 180^\circ = -1$ , which is evident in the difference between the exact and approximate solution. However, the difference is small enough to validate the approximation of spherical spreading in the near field of the bubble.

## References

- [1] Kerry W. Commander and Andrea Prosperetti. Linear pressure waves in bubbly liquids: Comparison between theory and experiments. *J. Acoust. Soc. Am.*, **85**:732–746, 1989.
- [2] T. K. Stanton. Multiple scattering with applications to fish-echo processing. *J. Acoust. Soc. Am.*, **73**:1164–1169, 1983.
- [3] Natalia Gorska and Zygmunt Klusek. Dependence of scattered acoustical signal intensity on the form of distribution of plankton concentration. *J. Acoust. Soc. Am.*, **104**:141–145, 1998.
- [4] N. de Jong, F. J. Ten Cate, C. T. Lancée, J. R. T. C. Roelandt, and N. Bom. Principles and recent developments in ultrasound contrast agents. *Ultrasonics*, **29**:324–330, 1991.
- [5] K. K. Shung, R. A. Sigelmann, and J. M. Reid. Scattering of ultrasound by blood. *IEEE Trans. Biomed. Eng.*, **BME-23**:460–467, 1976.
- [6] Philip M. Morse and Uno K. Ingard. *Theoretical Acoustics*. McGraw-Hill, New York, 1968.
- [7] J. Szczucka. Numerical model of multiple sound scattering from gas bubbles in the sea. *Arch. Acoust.*, **20**:191–205, 1995.
- [8] Irina Bjørnø and Leif Bjørnø. Numerical modelling of multiple scattering between two elastic particles. In *OCEANS'98 Conference Proceedings*, pages 598–602. IEEE/OES, New Jersey, 1998.
- [9] Leslie L. Foldy. The multiple scattering of waves. I. General theory of isotropic scattering by randomly distributed scatterers. *Phys. Rev.*, **67**:107–119, 1945.
- [10] A. Sangani. A pairwise interaction theory for determining the linear acoustic properties of the dilute bubble liquids. *J. Fluid Mech.*, **232**:221–284, 1991.

- [11] Zhen Ye and Li Ding. Acoustic dispersion and attenuation relations in bubbly mixture. *J. Acoust. Soc. Am.*, **98**:1629–1636, 1995.
- [12] Frank S. Henyey. Corrections to Foldy’s effective medium theory for propagation in bubble clouds and other collections of very small scatterers. *J. Acoust. Soc. Am.*, **105**:2149–2154, 1999.
- [13] Victor Twersky. Multiple scattering of waves and optical phenomena. *J. Opt. Soc. Am.*, **52**:145–171, 1962.
- [14] I. Tolstoy. Superresonant systems of scatterers. I. *J. Acoust. Soc. Am.*, **80**:282–294, 1986.
- [15] I. Tolstoy. Erratum: “Superresonant systems of scatterers. I”. *J. Acoust. Soc. Am.*, **81**:1987, 1987.
- [16] G. C. Gaunaurd, H. Huang, and H. C. Strifors. Acoustic scattering by a pair of spheres. *J. Acoust. Soc. Am.*, **98**:495–507, 1995.
- [17] Richard D. Mattuck. *A Guide to Feynman Diagrams in the Many-Body Problem*. Dover Publications, New York, 1992.
- [18] Victor C. Anderson. Sound scattering from a fluid sphere. *J. Acoust. Soc. Am.*, **22**:426–431, 1950.
- [19] Charles Devin, Jr. Survey of thermal, radiation, and viscous damping of pulsating air bubbles in water. *J. Acoust. Soc. Am.*, **31**:1654–1667, 1959.
- [20] Clarence S. Clay and Herman Medwin. *Acoustical Oceanography: Principles and Applications*. Wiley, New York, 1977.
- [21] Louis R. Dragonette, Richard H. Vogt, Lawrence Flax, and Werner G. Neubauer. Acoustic reflection from elastic spheres and rigid spheres and spheroids. II. Transient analysis. *J. Acoust. Soc. Am.*, **55**:1130–1137, 1974.

- [22] Irene A. Stegun. Legendre functions. In Milton Abramowitz and Irene A. Stegun, editors, *Handbook of Mathematical Functions*. U.S. Government Printing Office, 1972.
- [23] James J. Faran, Jr. Sound scattering by solid cylinders and spheres. *J. Acoust. Soc. Am.*, **23**:405–418, 1951.
- [24] Robert Hickling. Analysis of echoes from a solid elastic sphere in water. *J. Acoust. Soc. Am.*, **34**:1582–1592, 1962.
- [25] Kenneth G. Foote. Optimizing copper spheres for precision calibration of hydroacoustic equipment. *J. Acoust. Soc. Am.*, **71**:742–747, 1982.
- [26] Timothy G. Leighton, David G. Ramble, and Andy D. Phelps. The detection of tethered and rising bubbles using multiple acoustic techniques. *J. Acoust. Soc. Am.*, **101**:2626–2635, 1997.
- [27] F. H. Fisher and V. P. Simmons. Sound absorption in sea water. *J. Acoust. Soc. Am.*, **62**:558–564, 1977.
- [28] R. Clift, J. R. Grace, and M. E. Weber. *Bubbles, Drops, and Particles*. Academic Press, New York, 1978.
- [29] Michael S. Longuet-Higgins, Bryan R. Kerman, and Knud Lunde. The release of air bubbles from an underwater nozzle. *J. Fluid Mech.*, **230**:365–390, 1991.
- [30] Lawrence E. Kinsler, Austin R. Frey, Alan B. Coppens, and James V. Sanders. *Fundamentals of Acoustics*. Wiley, New York, 1982.
- [31] R. L. Pritchard. Mutual acoustic impedance between radiators in an infinite rigid plane. *J. Acoust. Soc. Am.*, **32**:730–737, 1960.
- [32] Sigeo Sugimoto, Akio Hasegawa, and Toshiaki Kikuchi. Active sound power reduction based on mutual radiation impedance effect between transducers in water. *Jpn. J. Appl. Phys.*, **33**:3294–3299, 1994.

# REPORT DOCUMENTATION PAGE

Form Approved  
OMB No. 0704-0188

Public reporting burden for this collection of information is estimated to average 1 hour per response, including the time for reviewing instructions, searching existing data sources, gathering and maintaining the data needed, and completing and reviewing the collection of information. Send comments regarding this burden estimate or any other aspect of this collection of information, including suggestions for reducing this burden to Washington Headquarters Services, Directorate for Information Operations and Reports, 1215 Jefferson Davis Highway, Suite 1204, Arlington, VA 22202-4302, and to the Office of Management and Budget, Paperwork Reduction Project (0704-0188), Washington, DC 20503

1. AGENCY USE ONLY (Leave Blank)		2. REPORT DATE 3 March 2000		3. REPORT TYPE AND DATES COVERED Final (10/1/95 - 12/31/98)	
4. TITLE AND SUBTITLE Effects of Interaction Between Two Bubble Scatterers				5. FUNDING NUMBERS N00014-96-1-0122	
6. AUTHOR(S) George Kapodistrias and Peter H. Dahl					
7. PERFORMING ORGANIZATION NAME(S) AND ADDRESS(ES) Applied Physics Laboratory University of Washington 1013 NE 40th St. Seattle, WA 98105-6698				8. PERFORMING ORGANIZATION REPORT NUMBER	
9. SPONSORING/MONITORING AGENCY NAME(S) AND ADDRESS(ES) Office of Naval Research 800 N. Quincy St. Arlington, VA 22217-5660 Attn: Dr. Jeffrey Simmen, Code 3210A				10. SPONSORING/MONITORING AGENCY REPORT NUMBER	
11. SUPPLEMENTARY NOTES  Report was accepted on March 3, 2000, for publication in the Journal of the Acoustic Society of America.					
12a. DISTRIBUTION/AVAILABILITY STATEMENT  Approved for public release				12b. DISTRIBUTION CODE	
13. ABSTRACT (Maximum 200 words) The backscattering of sound from two regularly arranged bubbles is studied theoretically and experimentally. In well controlled laboratory experiments a bistatic acoustic system is used to interrogate the scatterers, which are placed on a very fine thread at the same distance $d$ from the combined beam axis of the set of transmitting and receiving transducers. The radius of each bubble is $585 \mu m$ . The frequency range is 80-140 kHz, and $d$ is varied so that the variable $kd$ spans the range 0.2-21, where $k$ is the acoustic wavenumber. Scattering calculations are carried out using an exact, closed-form solution derived from the multiple scattering series. Several experiments are performed, and the results are in close agreement with the calculations. It is verified that multiple scattering induces an oscillatory behavior about the exact coherent scattering level, with decreasing amplitude for increasing $kd$ . For interbubble distance $2d \approx \lambda/2$ the backscattered radiation is maximized, while for $2d < \lambda/2$ the radiation is reduced considerably.					
14. SUBJECT TERMS  acoustic scatter from bubbles, multiple scattering				15. NUMBER OF PAGES 29	
				16. PRICE CODE	
17. SECURITY CLASSIFICATION OF REPORT Unclassified		18. SECURITY CLASSIFICATION OF THIS PAGE Unclassified		19. SECURITY CLASSIFICATION OF ABSTRACT Unclassified	
				20. LIMITATION OF ABSTRACT UL	

2000404001